
ELSEVIER

Nuclear Instruments and Methods in Physics Research B 166–167 (2000) 903–912

NIM B
Beam Interactions with Materials & Atoms

www.elsevier.nl/locate/nimb

Transient thermal processes in heavy ion irradiation of crystalline inorganic insulators

M. Toulemonde [a,*], Ch. Dufour [b], A. Meftah [c], E. Paumier [b]

[a] *CIRIL, Laboratoire CEA-CNRS-ISMRa, BP 5133, 14070 Caen Cedex 05, France*
[b] *LERMAT-ISMRa, Université de Caen, B[d] Du Maréchal juin, 14050 Caen Cedex, France*
[c] *LIRM, ENSET, BP 26, Merdj-eddib, 21000 Skikda, Algeria*

Abstract

A review of matter transformation induced in crystalline inorganic insulators by swift heavy ions is presented. The emphasis is made on new results obtained for amorphizable materials such as $Gd_3Ga_5O_{12}$, GeS, and $LiNbO_3$ and for non-amorphizable crystals such as SnO_2, LiF and CaF_2. Assuming that latent tracks result from a transient thermal process, a quantitative development of a thermal spike is proposed. The only free parameter is the electron–lattice interaction mean free path λ. With this parameter it is possible to quantitatively describe track radii, whatever the bonding character of the crystal is, in a wide range of ion velocities assuming two specific criteria: tracks may result from a rapid quenching of a cylinder of matter in which the energy deposited on the lattice has overcome either the energy necessary to reach a quasi-molten phase in the case of amorphizable materials or the cohesion energy in the case of non-amorphizable materials. The evolution of the λ parameter versus the band gap energy of the considered insulator will be presented. On the basis of this discussion some predictions are developed.

PACS: 61.80.J; 79.20.N; 81.40.G
Keywords: Ion irradiation; Tracks; Insulators; Thermal spike

1. Introduction

In order to face the challenge of describing the basic mechanism which governs the transfer of the energy deposited by the swift heavy ions on the target electrons to the atomic network, one has to consider the experimental results in various conditions of irradiations and in various insulators exhibiting a wide palette of physical properties. Since the experiment of Silk and Barnes [1], a lot of different insulators have been irradiated by swift heavy ion or cluster beams in the electronic stopping power regime (see [2–5]). Concerning any model for track formation, it becomes very clear that several aspects [5–10] must be taken into account:

1. The electronic properties of the irradiated materials play an important role: it is all the more

* Corresponding author. Tel.: +33-231-454-704; fax: +33-231-454-714.
E-mail address: m.toulemonde@ganil.fr (M. Toulemonde).

0168-583X/00/$ - see front matter
PII: S0168-583X(99)00799-5

easier to create latent tracks if the intrinsic electrical resistivity is high [5,8–10].
2. The amorphization of a two-component system [11] has been studied versus the ionicity bonding and it appears that the core track damage efficiency in amorphizable materials is bigger than in non-amorphizable ones (track radii in α-SiO_2 quartz [12,13] are larger than in LiF [14]).
3. The initial spatial distribution of the energy deposition on the electrons [15] is important: for a given value of the electronic stopping power (dE/dx), high projectile velocity induces a large radial distribution of the energy deposited on the electrons resulting in a small track radius due to the lower energy density [16].

Several models have been suggested [17–22] but up to now quantitative descriptions need several adjustable parameters. Furthermore, no link is put forward between these free parameters and any physical property of the irradiated materials.

This paper attempts to demonstrate that a complete development of the thermal spike model [23–28] is able to give a quantitative description of track formation in solids in the electronic stopping power regime independent of their metallic or insulating character, or their ionic or covalent bonding nature, by using only one free parameter: the mean free path of the electron–lattice interaction that can be linked to the band gap energy of the considered material.

2. Why to develop the thermal spike model?

Since the beginning of the 1950s, several theoretical models (e.g. Coulomb spike [17], thermal spike [18–21] or exciton [22] models) have been proposed to explain the appearance of tracks induced in matter by the slowing down of energetic ions in the electronic stopping power regime. But nowadays, the formation process is still not completely understood and relevant processes are controversially discussed.

In the Coulomb spike model [17], it is assumed that an energetic ion along its path creates a cylindrical region of highly ionized matter. Repulsive electrostatic forces act during the period before electronic neutrality is restored and give rise to a violent explosion within a time of 10^{-14}–10^{-13} s. This phenomenon leads to a localized destruction of the lattice. However, the development of a detailed and quantitative model based on such mechanism is difficult and is still not performed nowadays.

The thermal spike model [18–28] uses a different approach. Here the energy is deposited on the electrons of the target by the projectile. In a first step this energy is shared between electrons and, in a second step, is transferred to the lattice atoms by electron–lattice interaction leading to a large increase of temperature along the ion path. It has been shown that the thermal spike model can describe defect creation in metals by assuming that the damage results from the quenching of molten matter along the ion path [23,24]. Even several observations, such as the defect annealing [25], track formation [26], the effect of irradiation temperature [27] quantitatively support this description.

In the following, a slightly modified version of the thermal spike model [28] will be applied to insulators particularly oxides and ionic crystals. As the electron–lattice coupling is stronger in insulators [29] than in metals, a large increase of temperature along the ion trajectory is expected.

3. Mathematical description

3.1. Definition of the parameters

The thermal spike model is described mathematically by two coupled equations [30] governing the energy diffusion into the electron subsystem and into the lattice subsystem. A time-dependent transient thermal process coupling these two systems is expressed using a cylindrical geometry whose axis is the ion path:

$$C_e \frac{\partial T_e}{\partial t} = \nabla(K_e \nabla T_e) - g(T_e - T) + B(r,t),$$

$$\rho C(T) \frac{\partial T}{\partial t} = \nabla(K(T)\nabla T) + g(T_e - T),$$

where T_e, T, C_e, $C(T)$ and K_e, $K(T)$ are the temperature, the specific heat and the thermal con-

ductivity of the electronic and atomic systems, respectively. ρ is the specific mass of the lattice and g is the electron–phonon coupling constant [30]. $B(r,t)$, described previously [23,24,28], is the energy density supplied by the incident ion to the electronic system by ballistic collisions [15,31,32] at radius r and time t. The integration of $B(r,t)$ over time and space gives the total dE/dx [33].

The thermal parameters C_e and K_e of the electronic subsystem are unknown for insulators. Hence some assumptions must be made. Baranov et al. [34] suggested that hot electrons in the conduction band of an insulator behave like hot electrons in a metal. In that case, the free electron gas model can be applied leading to a value of the specific heat C_e which depends on the number (N_e) of electrons which participate in the energy diffusion: $C_e = \frac{3}{2} N_e k_B$ where k_B is the Boltzmann constant. Assuming an electron density of approximately 5×10^{22} e cm^{-3}, the C_e value is equal to 1 J cm^{-3} K^{-1} [35]. The thermal conductivity is linked to thermal diffusivity by the relation $K_e = D_e C_e$. In the free electron gas model $D_e = (1/3)\ell v_f$ where ℓ is the electron–electron mean free path and v_f the Fermi velocity (around 10^8 cm s^{-1}). This relation describes quite well the energy diffusion on the electrons at room temperature in a noble metal like gold [35,36] by using an ℓ value of 40 nm. At high electronic temperature, using a minimum value of ℓ equal to the interatomic distance, the relation leads to $D_e = 2$ cm^2 s^{-1}. Then knowing C_e and D_e, the thermal conductivity K_e is equal to 2 J cm^{-1} s^{-1} K^{-1}. These values are constant and identical for all the following calculations.

The electron–phonon coupling constant g is unknown in insulators. Howewer, g is expected to be larger for ionic crystals (like LiF...) than for covalent ones (like Si...) [37]. g is linked to the electron–lattice interaction time τ_a by the relation $\tau_a = C_e/g$ [28] and to the electron–lattice interaction mean free path λ by the relation $\lambda^2 = D_e\tau_a = D_e C_e/g = K_e/g$. In the present calculation, λ will be the only free parameter. In order to emphasize the insulating character of the materials considered here, the coupling constant, g, will be set to zero when the electron temperature becomes less than the lattice temperature.

The two coupled equations are numerically solved to take into account the temperature dependence of the lattice thermodynamical parameters as well as the "solid–liquid" and "liquid–vapor" phase changes. As previously done, all the lattice thermodynamical parameters [12,13,28,35] are taken from equilibrium measurements.

The effects of the electronic stopping power are nonlinear and appear above a threshold value of dE/dx. For example, for $Y_3Fe_5O_{12}$, tracks appear above 4 keV nm^{-1} [16] and the sputtering above 16 keV nm^{-1} [38]. Then, from the thermodynamical point of view, one has to define two possible criteria:

1. The energy ΔH_m [23,24] necessary to reach the molten phase. This energy includes both the heat quantity to raise the temperature from the irradiation temperature (T_0) to the melting temperature (T_m) plus the latent heat of fusion (L_m).
2. The energy ΔH_v necessary to reach the vapor phase. This energy includes ΔH_m plus the heat quantity to raise the temperature from T_m to the vaporization temperature (T_v) and the latent heat of vaporization. The energy ΔH_v corresponds to the sublimation energy (or the cohesion energy).

3.2. Application of the model to α-SiO_2 quartz

3.2.1. Track formation

The main output of the code is presented in Fig. 1 for α-SiO_2 quartz. It is the temperature evolution versus time for different shells around the ion trajectory. As previously quoted [39], below 10^{-13} s, the temperature should be considered as an energy deposited in the lattice: it is a "quasi-temperature". For longer time it can be considered as true temperature. Assuming that the track which corresponds to the transition to an amorphous phase in α-SiO_2 quartz results from the quenching of a liquid phase (the melting temperature T_m is 1972 K [12]), the calculated latent track radius is 5.5 nm in the presented case (Fig. 1). With the same criterion, a λ value of 4 nm is determined by fitting all the experimental radii [12,13] and, for this λ value and for a specific range of beam energy, the calculated track radii are reported in

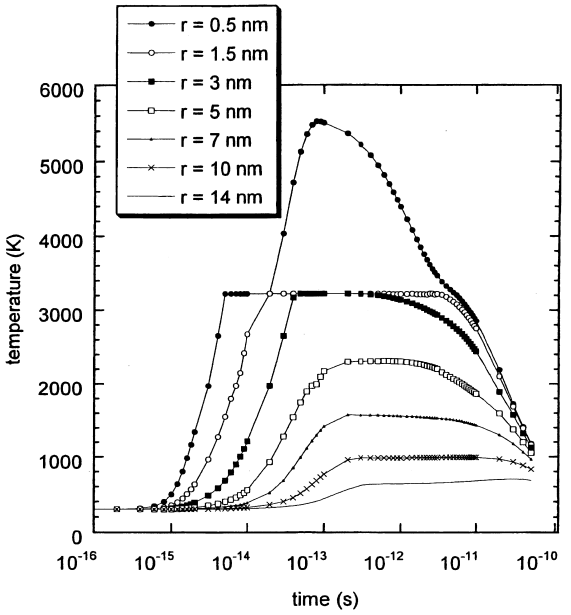

Fig. 1. Temperature evolution at different radial distances (inset in nanometers) from the ion axis in α-SiO_2 quartz. Melting temperature is $T_m = 1972$ K and vaporisation temperature is $T_v = 3223$ K. The initial temperature is 300 K, the beam energy 1.3 MeV/amu and the $dE/dx = 22$ keV/nm.

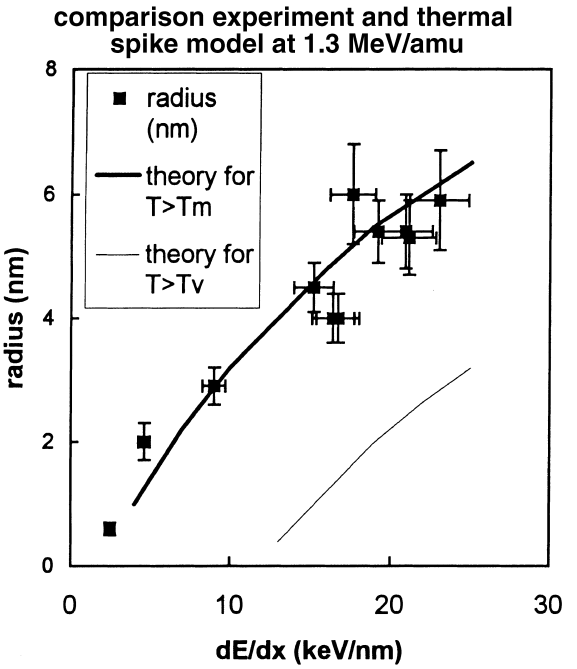

Fig. 2. Comparison for α-SiO_2 quartz of the thermal spike calculation ($\lambda = 4$ nm, a beam energy of 1.3 MeV/amu, a criterion of $T > T_m$ and temperature of irradiation of 300 K) and the experimental radii resulting from irradiation performed between 0.6 and 1.7 MeV/amu [12,13]. The second curve corresponds to cylinder of matter which overcomes the temperature of vaporization (T_v) for the same value of λ (see Section 3.2.2).

Fig. 2 (the curve labeled $T > T_m$). The calculation implies the creation of a continuous cylindrical track whose radius can be compared to the experimental effective radius which has been defined previously [16]. In order to discard the influence of the projectile velocity, we have reported in Fig. 2 the experimental radii for a specific energy range (see Section 3.3). The whole data set of radii [12,13,28] can be fitted using the same $\lambda = 4$ nm value whatever is the beam energy. With this value of λ, the electron–lattice interaction time τ_a is equal to 80×10^{-15} s which is in quite good agreement with the time of the energy relaxation determined by low power femtosecond laser experiments [40].

3.2.2. Electronic sputtering

Besides modeling the size of the tracks, the thermal spike model was applied to describe a sputtering experiment in the electronic energy loss regime [41]. In the present case, the sputter yield was calculated using a model derived from statistical thermodynamics [42,43]. The sputtering yield of Si from α-SiO_2 quartz, assuming the temperature given by the thermal spike, is presented in Fig. 3. For the calculation it was assumed that the planar surface potential used in the model corresponds to the sublimation energy. It should be noted that, with the same value ($\lambda = 4$ nm), the model can describe the experimental Si sputtering yield from α-SiO_2 quartz [41] as well as the evolution of track radii [12,13,28].

In Fig. 2 for the same λ value, the calculated radii are also illustrated versus dE/dx for a cylinder in which the temperature overcomes the vaporization temperature or the cohesion energy ($T > T_v$). By comparison with Fig. 3 one can see that huge sputtering appears when the vaporization temperature is surpassed at the surface, i.e., for dE/dx larger than 13 keV/nm.

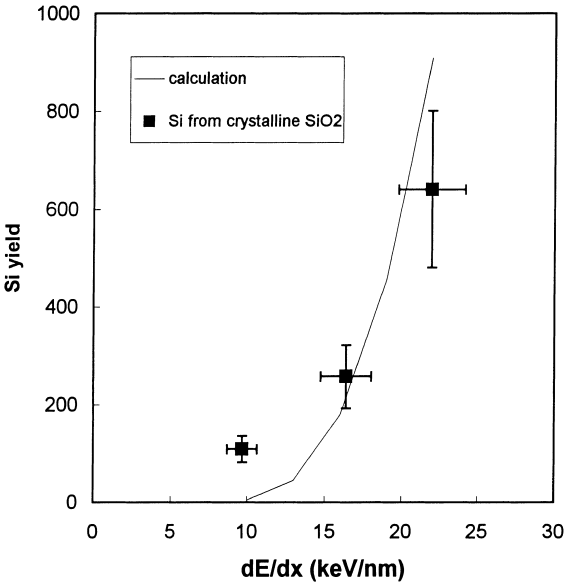

Fig. 3. Comparison for α-SiO_2 quartz of Si sputtering yield: the line corresponds to the thermal spike calculation and the points to the experiment.

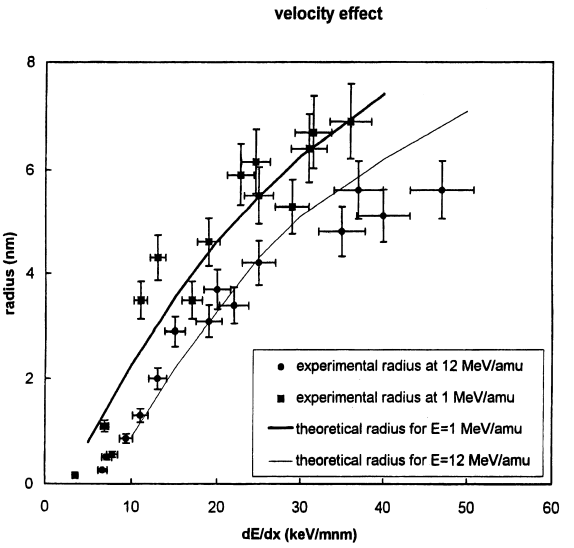

Fig. 4. Velocity effect in $Y_3Fe_5O_{12}$: comparison of the thermal spike calculation (lines) with experimental radii [16] measured in two specific beam energy ranges: around 1 MeV/amu and around 12 MeV/amu.

3.3. Application of the model to explain the velocity effect

In this model, one can estimate the effect of the ion beam velocity [15]. This was done in $Y_3Fe_5O_{12}$ for which a large set of data is available [16]. A λ value of 5 nm was determined from fitting the radii measured in a specific beam energy range (in the present case at around 1 MeV/amu) [44] using as an input the analytical formula proposed by Waligorski et al. [15] to describe the initial energy distribution deposited on the electrons. Then, using the same λ value, the radii versus dE/dx are calculated either for the case of beam energy being larger than 12 MeV/amu (Fig. 4) [44] or for the case of cluster irradiations [44,45]. The very good agreement shows the capability of the present modeling to take into account the effect of the projectile velocity.

4. Discussion: λ evolution versus energy band gap

Due to the limited space, we cannot present in detail all the calculations performed for various insulators. this will be done in two forthcoming papers [41,46]. However we shall present λ values deduced from a large series of data fits using a material classification: (1) amorphizable materials (Section 4.1) and (2) non-amorphizable materials (Section 4.2). Two peculiar cases (Al_2O_3 and vitreous silica) will be discussed in Section 4.3. Then these λ values will be discussed following the description made by Katin et al. [47] to explain the electron energy relaxation in insulators: they proposed that the energy dissipation in the electronic system proceeds via the ionization of bound electrons at the periphery of the excited region. The energy stops spreading when the electron energy becomes smaller than the minimum ionization energy. Consequently there should exist a link between the λ values and the band gap energy E_g which is the minimum ionization energy of an electron in insulators.

4.1. Amorphizable materials

As for α-SiO_2 quartz, it is assumed that the observed amorphous tracks result from the

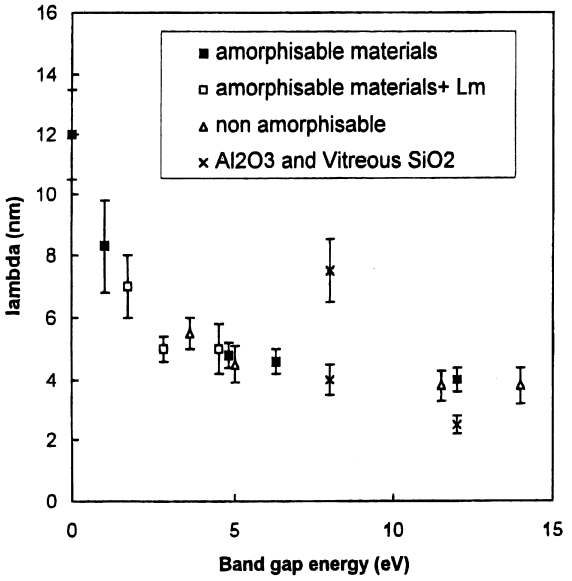

Fig. 5. Electron–lattice interaction mean free path λ versus the band gap energy E_g. Two possible values of λ are reported for Al_2O_3 (see Section 4.3).

quenching of a molten matter. A large data set is available [12,13,16,28,44,48–52]. These materials were studied by Meftah [53] and the λ values, deduced from fitting the track radii, are reported in Fig. 5 for materials for which all the thermodynamical parameters are known: SiO_2 ($E_g = 12$ eV) [12,13,28], $Y_3Al_5O_{12}$ ($E_g = 6.3$ eV) [48], $Gd_3Ga_5O_{12}$ ($E_g = 4.8$ eV) [53], $BaFe_{12}O_{19}$ ($E_g = 1$ eV) [28] and $YBa_2Cu_3O_{6.9}$ ($E_g \approx 0$ eV) [49].

For some materials which are amorphizable like $LiNbO_3$ ($E_g = 4.8$ eV) [50,51] and GeS ($E_g = 1.7$ eV) [52], the latent heat of fusion (L_m) is unknown. In these cases, the latent heat of fusion is also included as a second parameter and, from the fitting procedure, a unique set of λ and latent heat of fusion values [53] can be extracted. Moreover, $Y_3Fe_5O_{12}$ has no congruent melt phase so that L_m cannot be measured. But the heating of the matter in the case of ion irradiation is so rapid that we can assume a value for the latent heat of fusion and also extract a unique set of values for L_m and λ [44]. The deduced λ values are reported in Fig. 5.

Fig. 5 shows the λ values versus the band gap energy E_g for all amorphizable materials. It is interesting to notice that the suggestion of Katin et al. [47] leads to a direct correlation between E_g and λ. For E_g larger than 2.8 eV, there is only a slight decrease of λ (from 5 to 4 nm), suggesting that crystalline insulators behave nearly in the same way concerning the electron energy transfer towards the atoms [20,21].

4.2. Non-amorphizable materials

For crystals with mainly ionic bonding character [11], amorphization is not expected. However, it is interesting to note that in these kinds of materials tracks exist [14,54]. The first observation made in LiF [14] shows that the track radii are systematically lower than those extracted for amorphizable materials: this fact is illustrated by the comparisons that can be made on one hand between LiF [14] and mica [55] using the same physical characterization (small angle X-rays scattering) and on the other hand between CaF_2 [54] and $Y_3Fe_5O_{12}$ [16,45] using transmission electron microscopy. Such comparisons indicate that these non-amorphizable materials with a very strong electron–phonon coupling [37] are less damaged than the amorphizable ones. Recent experimental result of tracks in SnO_2 possibly gives an answer to this apparent contradiction [56].

Hémon et al. and Berthelot et al. [56,57] have studied the sensitivity of the tin oxide under swift heavy ion irradiation. Contrary to previous expectations [11], they did not observe the amorphization of the tin oxide. This may be specific of the single impact damage creation in the electronic energy loss regime. But holes have been evidenced by transmission electron microscopy corresponding to zones from which the material has been sputtered off. The authors proposed to link the size of the hole to a cylinder radius in which the sublimation energy has been exceeded. Then fitting the hole radii with this criterion (ΔH_v or a temperature larger than the vaporization temperature), they extract a λ value of 5.5 nm. With a band gap of 3.6 eV, this material follows the trend shown in Fig. 5.

A detailed study of CaF_2 ($E_g = 11.5$ eV) [46,54] leads also to the same conclusion: as shown in Fig. 6, it is impossible to describe the evolution of

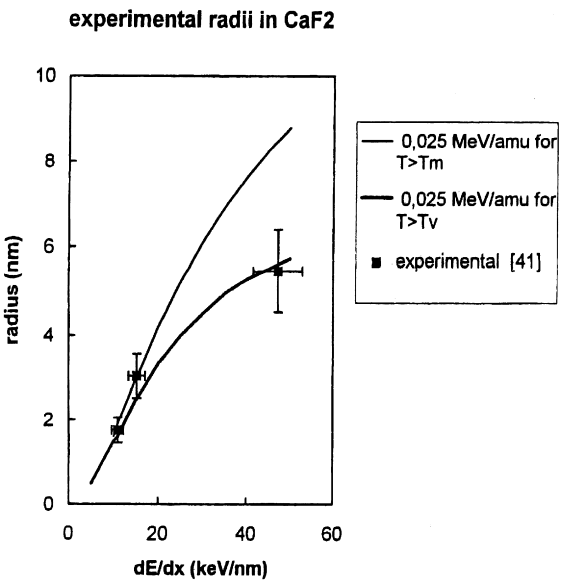

Fig. 6. Two calculations for CaF_2: cylinder of matter which overcomes the energy necessary to melt ($T > T_m$) with $\lambda = 8$ nm and cylinder of matter which overcomes the cohesion energy ($T > T_v$) with $\lambda = 3.8$ nm.

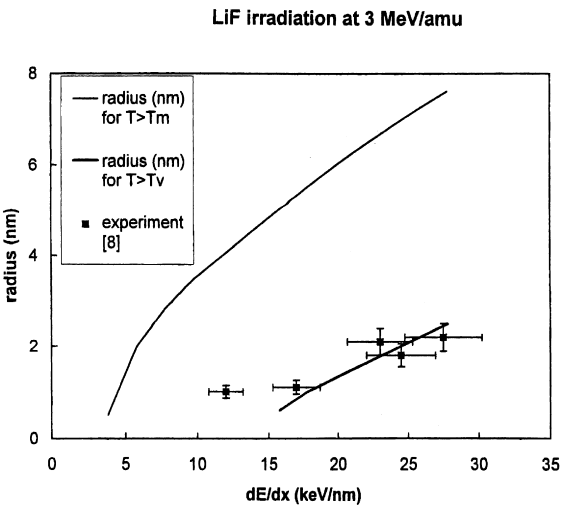

Fig. 7. Comparison between experiment and thermal spike calculation for LiF at 3 MeV/amu.

track radii assuming that the tracks are formed from the quenching of a molten phase. But if we assume that these tracks correspond to a cylinder of matter in which the energy deposited on the lattice surpassed the cohesion energy, one can extract a λ value of 3.8 nm.

For SnO_2 and CaF_2, λ versus E_g follows the same tendency as in the case of amorphizable materials (Fig. 5) with the following difference: in non-amorphizable materials the tracks, observed by transmission electron microscopy, are described by a cylindrical zone that has received an energy larger than the sublimation energy near the surface or the cohesion energy in the bulk, respectively.

Applying the same criterion to LiF ($E_g = 14$ eV) [14] with $\lambda = 3.8$ nm, one can follow quantitatively the track radii observed by small angle X-rays scattering (Fig. 7). Now, with the same value of λ and with a beam energy of 3 MeV/amu, the thermal spike model predicts that a melt phase should appear above a dE/dx value of 4 keV/nm leading to a track radius as large as 7 nm at $dE/dx = 25$ keV/nm. It is surprising to see that this later calculated radius (Fig. 7) is in agreement with the one extracted from swelling measurements in LiF [58], indicating that the appearance of the melt phase along the ion path can induce a specific change in the irradiated non-amorphizable material.

Experimental track data are also available for UO_2. These tracks were modeled previously with a λ value of 6 nm assuming the appearance of a molten phase [59]. The description given above for non-amorphizable materials dictates us to revise the previous calculation [59] and to use the cohesion energy criterion for track formation in this material. In that case a λ value of 4 nm can be extracted to fit the latent track observations [59], exhibiting the same good agreement as previously. A new experiment shows that a large sputtering yield due to the electronic excitation was measured in UO_2 [60] [1] for a dE/dx higher than 20 keV nm^{-1}. By comparison with SiO_2 quartz, this observation suggests that the sublimation energy has been surpassed in a large cylindrical track, supporting the $\lambda = 4$ nm assumption. Moreover such a λ value should support the observation of large surface tracks in UO_2 [61] at a lower dE/dx value

[1] The measured sputtering yield seems to be 2 order of magnitude too large and an explanation will be given in forthcoming paper.

than the one used by Wiss et al. [59]. This ambiguity in the determination of the λ value can also be removed if track radii are measured in a large range of dE/dx as demonstrated in the case of CaF_2.

In conclusion, it appears that, using the cohesion energy as the criterion to create observable tracks, these non-amorphizable materials follow the evolution of λ versus E_g (Fig. 5).

4.3. Two peculiar cases: Al_2O_3 and vitreous SiO_2

Sapphire with band gap of $E_g = 8$ eV [62,63] is difficult to classify as an amorphizable or a non-amorphizable material [11]. When fitting the experimental observations, two cases are possible [53]: either a λ value of 8 nm assuming the melt phase or a λ value of 4 nm in combination with the cohesion energy criterion. Indeed knowing the band gap energy of Al_2O_3, the correlation between λ and E_g, shown in Fig. 5, suggests that the track creation for dE/dx larger than 21 keV/nm would rather be associated to the cohesion energy (i.e. $\lambda = 4$ nm). This fact implies that a melt phase, which is not quenched into an amorphous phase and which surrounds the observed track core cylinder, should appear for dE/dx values lower than 21 keV/nm and above a threshold value of 8 keV/nm. The dE/dx-threshold of the appearance of this melt phase corresponds to an irradiation by Ar ions at an energy of 1 MeV/amu for which a peculiar evolution of point defect creation has been shown [64].

Finally we want to discuss the damage formation in vitreous silica. It has been demonstrated that all amorphous materials are sensitive to heavy ion irradiation [65]. Moreover it has also been demonstrated that the damage induced by swift heavy ion irradiation in amorphous materials is confined along the ion trajectory [66–68]. Assuming that tracks result from the quenching of molten matter, a λ value of 2.5 nm [69] was extracted. Moreover compaction of vitreous silica can be explained by the calculated large increase of temperature [70]. Using the same λ value, the Si sputtering rate was calculated by Meftah et al. [41] in agreement with the experimental observation [71]. The fact that this λ value does not follow the overall evolution in Fig. 5, may be explained by the initial amorphous state of the irradiated material. The interesting point is the determination of a different λ value as compared to the α-SiO_2 quartz ($\lambda = 4$ nm) leading to an electron lattice interaction time of 31 fs. This difference between the two phases of the SiO_2 has not been evidenced by fs laser irradiation [40,72] and is possibly a specific feature of the ion irradiation in the electronic stopping power regime.

5. Conclusion

Track formation has been analyzed in the framework of the thermal spike model in several kinds of inorganic solids, particularly in oxides and ionic crystals leading to the following coherent description:

1. In amorphizable materials, tracks appear when the energy necessary to melt is surpassed.
2. In non-amorphizable materials, track radii can only be described assuming that the cohesion energy is surpassed.
3. Sputtering appears when sublimation energy is reached.
4. The bonding character of the irradiated materials defines the specific behavior of the material under swift heavy ion irradiation.

With these two criteria 1 and 2, one can determine the electron–lattice interaction mean free path λ whatever the thermodynamical parameters of the lattice are. Moreover as suggested by Katin et al. [47] λ decreases as the band gap energy increases. The present interpretation of λ has to be compared to the observations made on the surface of same insulators irradiated by high and low power femtosecond laser [40,72,73].

References

[1] E.C.H. Silk, R.S. Barnes, Philos. Mag. 4 (1959) 970.
[2] Swift Heavy Ions in Matter conferences: SHIM 92, Radiat. Effects Defects Solids 126 (1993) 1.
[3] Swift Heavy Ions in Matter conferences: SHIM 95, Nucl. Instr. and Meth. B 107 (1996) 1.
[4] Swift Heavy Ions in Matter conferences: SHIM 98, Nucl. Instr. and Meth. B 146 (1998) 1.

[5] M. Toulemonde, F. Studer, Key Engin. Mat. 155–156 (1998) 267.
[6] F. Studer, M. Hervieu, J.M. Costantini, M. Toulemonde, Nucl. Instr. and Meth. B 122 (1997) 449.
[7] M. Toulemonde, S. Bouffard, F. Studer, Nucl. Instr. and Meth. B 91 (1994) 108.
[8] D. Bourgault, S. Bouffard, M. Toulemonde, D. Groult, J. Provost, F. Studer, N. Nguyen, B. Raveau, Phys. Rev. B 39 (1989) 6549.
[9] Y. Zhu, Z.X. Cai, R.C. Budhani, M. Suenaga, D.O. Welch, Phys. Rev. B 48 (1993) 6436.
[10] H.R. Kokabi, F. Studer, M. Toulemonde, Nucl. Instr. and Meth. B 11 (1996) 75.
[11] H.M. Naguib, R. Kelly, Radiat. Eff. 25 (1975) 1.
[12] A. Meftah, F. Brisard, J.M. Costantini, E. Dooryhee, M. Hage-Ali, M. Hervieu, J.P. Stoquert, F. Studer, M. Toulemonde, Phys. Rev. B 49 (1994) 12457.
[13] C. Trautmann, J.M. Costantini, A. Meftah, K. Schwartz, J.P. Stoquert, M. Toulemonde, Mat. Res. Symp. Proc. 504 (1998) 123.
[14] K. Schwartz, C. Trautmann, T. Steckenreiter, O. Geiss, M. Krämer, Phys. Rev. B 58 (1998) 11232.
[15] M.P.R. Waligorski, R.N. Hamm, R. Katz, Nucl. Tracks Radiat. Meas. 11 (1986) 309.
[16] A. Meftah, F. Brisard, J.M. Costantini, M. Hage-Ali, J.P. Stoquert, F. Studer, M. Toulemonde, Phys. Rev. B 48 (1993) 920.
[17] R.L. Fleisher, P.B. Price, R.M. Walker, Nuclear Tracks in Solids, University of California Press, California, 1975.
[18] G. Bonfiglioli, A. Ferro, A. Mojoni, J. Appl. Phys. 32 (1961) 2499.
[19] C.C. Watson, T.A. Tombrello, Rad. Eff. 89 (1985) 263.
[20] G. Szenes, Phys. Rev. B 51 (1995) 8026.
[21] G. Szenes, Phys. Rev. B 52 (1995) 6154.
[22] N. Itoh, A. Marshall, Nucl. Instr. and Meth. B 146 (1998) 362.
[23] Z.G. Wang, Ch. Dufour, E. Paumier, M. Toulemonde, J. Phys.: Condens. Matter 6 (1994) 6733.
[24] Z.G. Wang, Ch. Dufour, E. Paumier, M. Toulemonde, J. Phys.: Condens. Matter 7 (1995) 2525.
[25] Z.G. Wang, Ch. Dufour, E. Paumier, M. Toulemonde, Nucl. Instr. and Meth. B 115 (1996) 577.
[26] M. Toulemonde, Ch. Dufour, Z.G. Wang, E. Paumier, Nucl. Instr. and Meth. B 112 (1996) 26.
[27] Ch. Dufour, F. Beuneu, E. Paumier, M. Toulemonde, Europhys. Lett. 45 (1999) 585.
[28] M. Toulemonde, J.M. Costantini, Ch. Dufour, A. Meftah, E. Paumier, F. Studer, Nucl. Instr. and Meth. B 116 (1996) 37.
[29] R.F. Haglung, R. Kelly, Math. Phys. Medd. 43 (1993) 527.
[30] M.I. Kaganov, I.M. Lifshitz, L.V. Tanatarov, Sov. Phys. – JETP 4 (1957) 173.
[31] B. Gervais, S. Bouffard, Nucl. Instr. and Meth. B 88 (1994) 355.
[32] A. Miotello, R. Kelly, M. Dapor, Nucl. Instr. and Meth. B 141 (1998) 16.
[33] TRIM91 code, J.P. Biersack, L.G. Haggmark, Nucl. Instr. and Meth. 174 (1980) 257.
[34] I.A. Baranov, Yu.V. Martinenko, S.O. Tsepelevitch, Yu.N. Yavlinskii, Sov. Phys. Usp. 31 (1988) 1015.
[35] Ch. Dufour, A. Audouard, F. Beuneu, J. Dural, J.P. Girard, A. Hairie, M. Levalois, E. Paumier, M. Toulemonde, J. Phys.: Condens. Matter 5 (1993) 4573.
[36] Ch. Dufour, Z.G. Wang, M. Levalois, P. Marie, E. Paumier, F. Pawlak, M. Toulemonde, Nucl. Instr. and Meth. B 107 (1996) 218.
[37] W. Hayes, A.M. Stoneham, Defects and Defect Processes in Nonmetallic Solids, Wiley, New York, 1985.
[38] A. Meftah, M. Djebarra, J.P. Stoquert, F. Studer, M. Toulemonde, Nucl. Instr. and Meth. B 107 (1996) 242.
[39] M. Toulemonde, Ch. Dufour, E. Paumier, Phys. Rev. B 46 (1992) 14362.
[40] P. Audebert, Ph. Daguzan, A. Dos Santos, J.C. Gauthier, J.P. Geindre, S. Guizard, G. Harmoniaux, K. Krastev, P. Martin, G. Petite, A. Antonetti, Phys. Rev. Lett. 73 (1994) 1990.
[41] A. Meftah, S. Boudjadar, W. Assmann, H.D. Mieskes, C. Trautmann, M. Toulemonde, Unpublished results.
[42] P. Sigmund, C. Claussen, J. Appl. Phys. 52 (1981) 990.
[43] L.E. Seiberling, J.E. Griffith, T.A. Tombrello, Rad. Eff. 52 (1980) 201.
[44] A. Meftah, M. Djebara, N. Khalfaoui, M. Toulemonde, Nucl. Instr. and Meth. B 146 (1998) 431.
[45] J. Jensen, A. Dunlop, S. Della Negra, M. Toulemonde, Nucl. Instr. and Meth. B 146 (1998) 412.
[46] Ch. Dufour, Private communication.
[47] V.V. Katin, Yu.V. Martinenko, Yu.N. Yavlinskii, Sov. Techn. Phys. Lett. 13 (1987) 276.
[48] A. Meftah, M. Djebara, N. Khelfaoui, J.P. Stoquert, F. Studer, M. Toulemonde, Mat. Sci. Forum 248–249 (1997) 53.
[49] N. Khalfaoui, Ph.D. Thesis, University of Algier, Algeria, 1997.
[50] N. Bonardi, Ph.D. Thesis, University C. Bernard Lyon, France, 1998.
[51] B. Canut, S.M.M. Ramos, R. Brenier, P. Thevenard, J.L. Loubet, M. Toulemonde, Nucl. Instr. and Meth. B 107 (1996) 194.
[52] J. Vetter, R. Scholz, D. Dobrev, L. Nistor, Nucl. Instr. and Meth. B 141 (1998) 747.
[53] A. Meftah, Private communication.
[54] J. Jensen, A. Dunlop, S. Della Negra, Nucl. Instr. and Meth. B 141 (1998) 753.
[55] D. Albrecht, P. Armbruster, R. Spohr, M. Roth, K. Schaupert, H. Stuhrmann, Appl. Phys. A 37 (1985) 37.
[56] S. Hémon, F. Gourbilleau, Ch. Dufour, E. Paumier, E. Dooryhee, A. Rouanet, Nucl. Instr. and Meth. B 122 (1997) 526.
[57] A. Berthelot, F. Gourbilleau, C. Dufour, B. Domengès, E. Paumier, Nucl. Instr. and Meth. 166–167 (2000) 927.
[58] C. Trautmann, K. Schwartz, J.M. Costantini, T. Steckenreiter, M. Toulemonde, Nucl. Instr. and Meth. B 146 (1998) 367.

[59] T. Wiss, Hj. Matzke, C. Trautmann, M. Toulemonde, S. Klaumunzer, Nucl. Instr. and Meth. B 122 (1997) 583.
[60] S. Bouffard, J.P. Duraud, M. Mosbah, S. Schlutig, Nucl. Instr. and Meth. B 141 (1998) 372.
[61] C. Ronchi, J. Appl. Phys. 44 (1973) 3575.
[62] B. Canut, A. Benyagoub, G. Marest, A. Meftah, N. Moncoffre, S.M.M. Ramos, F. Studer, P. Thevenard, M. Toulemonde, Phys. Rev. B 51 (1995) 12194.
[63] S.M.M. Ramos, N. Bonardi, B. Canut, S. Bouffard, S. Della-Negra, Nucl. Instr. and Meth. B 143 (1998) 319.
[64] V.A. Skuratov, Nucl. Instr. and Meth. B 146 (1998) 385.
[65] S. Klaumünzer, G. Schumacher, Li. Changlin, S. Löffler, M. Rammensee, H.C. Neitzert, Rad. Eff. Def. Sol. 108 (1989) 131.
[66] C. Trautmann, S. Andler, W. Brüchle, R. Spohr, M. Toulemonde, Rad. Eff. Def. Sol. 126 (1993) 207.
[67] C. Trautmann, Ch. Dufour, E. Paumier, R. Spohr, M. Toulemonde, Nucl. Instr. and Meth. B 107 (1996) 397.
[68] A. Dunlop, G. Jaskierowicz, S. Della-Negra, C.R. Acad. Sci. Paris 325 (1997) 397.
[69] M. Toulemonde, Ch. Dufour, E. Paumier, F. Pawlak, Mat. Res. Soc. Symp. Proc. 504 (1998) 99.
[70] A. Benyagoub, S. Klaumünzer, M. Toulemonde, Nucl. Instr. and Meth. B 146 (1998) 449.
[71] J. Chaumont, H. Bernas, A. Kusnetsov, C. Clerc, L. Dumoulin, Nucl. Instr. and Meth. B 129 (1997) 436.
[72] A. Rosenfeld, D. Ashkenasi, H. Varel, M. Wähmer, E.E.B. Campbell, Appl. Surf. Sci. 127–129 (1998) 76.
[73] S. Guizard, C. Itoh, P. Martin, P. Meynadier, P. D'Oliviera, M. Perdrix, G. Petite, Nucl. Instr. and Meth. B 141 (1998) 66.